The Efficient and Stable Charging of Electric Vehicle Batteries: Simplified Instantaneous Regulation

Rui Medeiros, Stanimir Valtchev, Svilen Valtchev

HAL Id: hal-01365722
https://inria.hal.science/hal-01365722

Submitted on 13 Sep 2016

The Efficient and Stable Charging of Electric Vehicle Batteries: Simplified Instantaneous Regulation

Rui Medeiros[1], Stanimir Valtchev[1, 2], and Svilen Valtchev[3, 4]

[1]UNINOVA and [2]Dept. of Electrical Engineering, FCT/UNL, Portugal
[3]IP Leiria and [4]CEMAT of IST Lisboa, Portugal

Abstract. The future charging of the growing fleet of Electric Vehicles (EV) requires new solutions that guarantee a better efficiency and widely spread chargers. Both in fast charging and in slow charging of the electric vehicle (EV) and hybrid electric vehicle (HEV), the wireless charger is the better choice. The wired charger is limited by its cabling and relatively lower output voltage, while the contactless charger can be more universal and safe. What rests to be discovered is the more efficient energy transfer that would have a stable operation. The strategy is based on guaranteeing the correct portion of energy transported by the resonant tank to the load. Some results are shown from this implementation of the instantaneous energy control.

Keywords: Electric/Hybrid Vehicle, Battery, Charging, Contactless Energy Transfer, Series-Loaded Series-Resonant Converter

1 Introduction

The most problematic building block of any autonomous electric driven vehicle is its electric energy source. The battery defines the most important characteristics of the vehicle: the total available energy (i.e. its autonomy) together with the achievable velocity and acceleration (i.e. maximum instantaneous power).

   For example, the Li-Ion battery of 25kWh can guarantee 200km of autonomy but its weight is at least 150kg and costs at least 12000€. In parallel, a fuel tank of 50 litters will be sufficient for 900 or more km autonomy. The electric motor has advantages they are not sufficient to compensate for the battery disadvantages: heavy, expensive, short life, etc. The lack of suitable batteries is the reason for the HEV and Plug-in HEV to exist. In case of HEV and especially PHEV the battery is smaller and the speed (the power) of charging is usually limited to the household grid capacity. It is not easy to decide if fast or slow charging will be adopted. The internal combustion engine habits are strongly influencing the thinking of the consumer but it is predictable that a slower and more regular charging will be more efficient (lower power required, longer battery life, smart grids, etc.). The contactless charging is capable to offer higher power charging solutions but it is not so attractive to apply almost megawatt power to succeed in charging for 5 minutes. To make clearer how important is the speed and the depth of discharge of the battery, SAFT provided diagrams based on measurements on real EV batteries (Figs.1 and 2). Similar results are known for the charging of batteries.

The life expectancy of the battery (defined here as the moment when the capacity of the battery diminishes by 20%) is seen to be halved (Fig.1) if the depth of discharge of each cycle (DOD) changes from 50% to 80%, i.e. from 4900 charging/discharging cycles to 2300 cycles. The internal resistance is also doubled in the same number of cycles: slowly when the battery is treated by DOD = 50% and rapidly if DOD = 80%.
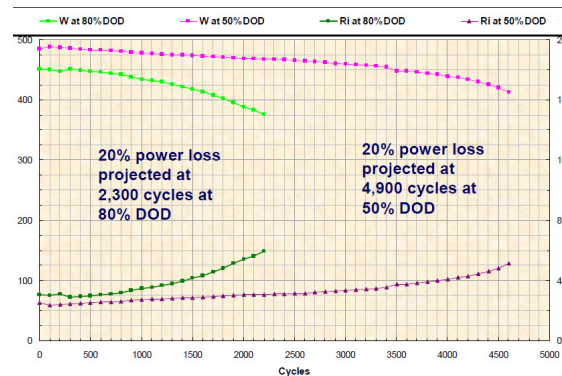

Fig. 1. Discharge Depth (80% and 50%) until 20% change in power and internal resistance
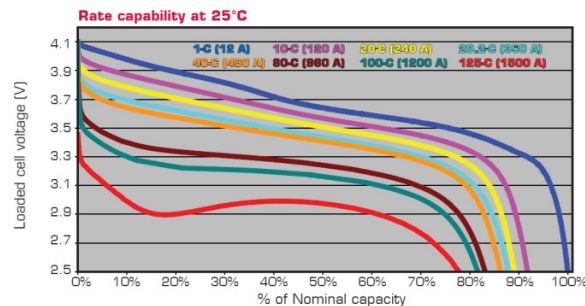

Fig. 2. Discharging at 1C (12 A) up to 125C (1500A), battery of SAFT Li-Ion VL45E cells

The available capacity of the battery, shown in Fig.2, is also becoming lower when high speed of discharge is applied (i.e. forcing the chemical processes). The curves in Fig.2 correspond also to Peukert's equation in general: the useable capacity diminishes if the charge/discharge currents go higher.

Another factor limiting the capabilities of the fast charging devices is the grid, which should in this case supply huge power levels in inconvenient place and time. To use the cars as energy storage in smart grids in case of fast charging is also improbable: high peaks of energy transfer are inconvenient.
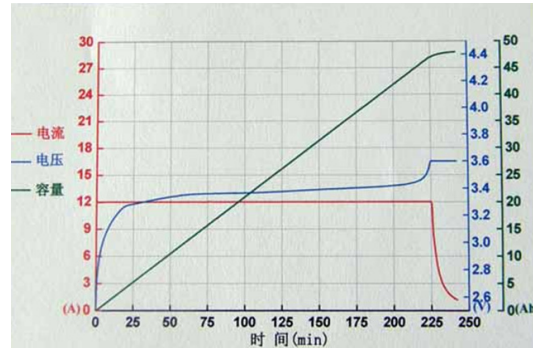
Fig. 3. Charging process curves of 40 Ah, SE40AHA battery (Sky Energy, China)

The slower (safer) charging station is supposed to use the pattern shown in Fig.3, where it is seen that the initial charging process runs at a fixed current of 12A, and later the current goes exponentially down while the voltage is kept constant.

2   Contribution to Value Creation

Many contributions were made in the last years to improve the efficiency and the controllability of the resonant converters [5,6,7]. The interest in wireless power transmission has been growing for the last two decades, especially because the technology is now advanced enough to implement it.

This work proposes a further improvement to the simplified method to control the energy transported by the resonant tank(s) to the load (EV battery), reported in [10]. This new Instantaneous Control is similar in its essence to the classic CM (Current-Mode) Control [11], but in the new method the internal variable used to control the resonant processes is the resonant capacitor voltage instead of the inductor current. The method proved to be valid in simulations [10], followed now in measurements. It appears simple, fast and efficient.

3   Contactless Charging

The transfer of the charge to the battery is the most important technological problem of the EV (or of some other autonomous, e.g., robotic device). This problem is closely connected to the speed of charge, to the feedback information from the battery, etc.

A solution could be to apply a wireless (e.g. Inductively Coupled) energy transfer where cables are not required and the secondary rectifier can be connected by fixed and better cooled copper bars. The wireless energy transfer is a credible solution for the charging as it permits a safer energy interface with the vehicle even during bad weather, careless manipulation, etc. The chargers can be aimed either at a static position of the EV in relation to the transmitter of energy, or to the dynamic position. For the moment, the static charger is expected to have wider penetration into the

market but the dynamic charging has some (the infrastructure is expensive and less efficient) support from the engineers. One example of dynamic charger is the OLAV project in Republic of Korea (Fig.4). The dynamic contactless power transfer is already applied in the industry, e.g. for robots at a fixed route.

Fig. 4. Street bus with dynamic charging by underground transmitters (KAIST, Korea)

In both its static and dynamic version, the contactless power transfer can be (in theory) bi-directional. This requires of course, a more sophisticated secondary side but makes possible the energy management of the grid.

4   The Series Resonant Topology for Contactless Charging

The main topologies for wireless energy transfer are always resonant. The versions may include one or two resonant loops, each one series or parallel, differing also by the way the load is connected. Here the main topology will be the series resonant converter although the other versions are kept in mind. This version involves a series connection of L and C elements and in terms of resonant frequency stability, this is the better solution. This resonant topology is characterized by higher amplitudes of the resonant current, which is not so difficult to cope with. The modern switching power devices have enough reserve in maximum allowed current value (the breakdown voltage is still a limitation, especially when low voltage drop and high speed at high current are required).

5   The Regulation of the Charge in a Resonant Topology

5.1 Energy Balance

An excitation voltage V_{LC} is applied to the series resonant loop LrCr and can be represented as the instantaneous difference between the input and output voltages v_s and v_o (Fig.6). In case of loosely connected magnetic link the same figure corresponds to the recalculated primary [1,9].
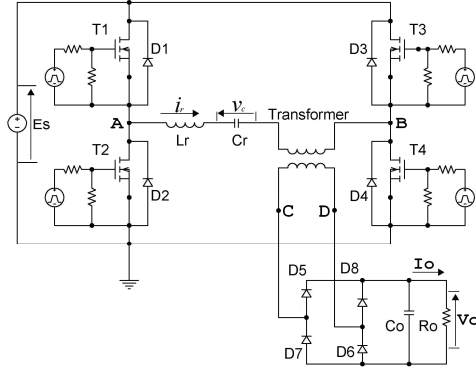
Fig. 5. DC-DC series resonant converter with transformer connection to the output rectifier
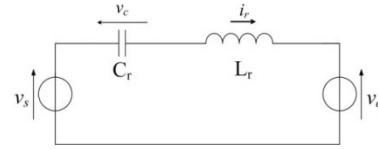
Fig. 6. Equivalent circuit of the simplified SLSR power converter

The excitation voltage V_{LC} applied across the LC tank ($v(C_r)+v(L_r)$) is $V_{LC1}>0$ during the interval ψ_1 (Fig.7) and $V_{LC2}<0$ in the interval ψ_2. In some equations and in Fig.8 (for convenience) the normalized (angular) variables ψ_1, ψ_2 and ωt, are substituted with the time variable t.

In a steady-state operation the energy $\Delta\mathscr{E}_{LC}$ of the LC tank equals zero in the beginning and the end of each half period of switching. The current increases from zero and charges energy to the tank until t_1 (Fig.8) and this energy is discharged after t_1 until the end of the half switching period:

$$\Delta\mathscr{E}_{LC} = \int_0^{t_1} V_{LC1} i_r dt + \int_{t_1}^{\frac{T_{sw}}{2}} V_{LC2} i_r dt = 0 \qquad (1)$$

The energy increase $\Delta\mathscr{E}_{LC}$ is defined as zero as the energy portion extracted from the input voltage source E_s is equal to the energy portion delivered to the output voltage source V_o. If it is necessary to increase the energy in the tank, then the circuit will be commanded by a longer conduction interval ψ_1 than the necessary for its steady state, and hence $\Delta\mathscr{E}_{LC}$ will be positive. When the energy must diminish, then ψ_1 is decreased and $\Delta\mathscr{E}_{LC}$ will be negative.

At the zero crossing points of the current (Figs.7,8) the total resonant tank energy consists only of resonant capacitor energy $\dfrac{C_r v_{cmax}^2}{2}$, so the capacitor voltage maximums v_{cmax} can be used to assess that energy [1].

$$\Delta\mathscr{E}_C^N(0,\frac{T_{sw}}{2}) = 2v_c(t_1) - q(v_{cmax1} + v_{cmax2}) \qquad (2)$$
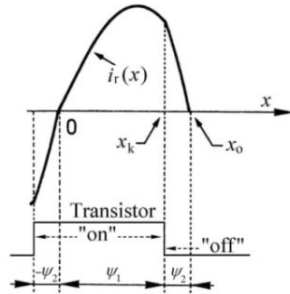
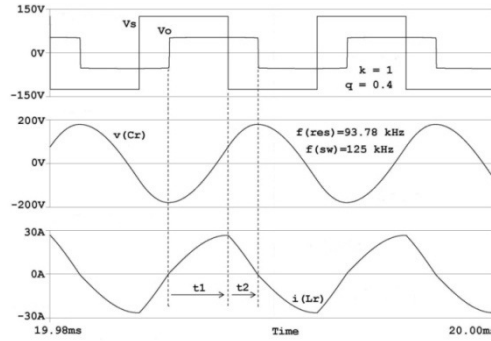**Fig. 7.** Resonant current i_r intervals and power switch command

Fig. 8. Super-resonant (FM) operation of SLSR converter

Expression (2) involves the capacitor voltage $v_c(t_1)$ at which the conducting switch (or the diagonal) is switched off (t_1 corresponds to the angular point x_k). The equation involves also the previously measured amplitude v_{cmax1} and the necessary next amplitude v_{cmax2} which may be different if it would be necessary to change the energy portion.

In the case of contactless power transfer, the converter operation is described by the same expression (2) where v_{cmax1} and v_{cmax2} correspond to the resonant capacitor voltage amplitudes in the primary [9]. In that case, the normalized output voltage q in (2) will be substituted by the corrected value $q^T = Kq$, where K is the magnetic coupling factor of the loosely coupled magnetic link (transformer).

5.2 Simplified Strategy for Regulation

In the hard switching converter with Current Mode regulation, the inductor current is the instantaneous power indicator for the energy transferred each half period in the SLSR converter. Considering that the resonant processes are not so simple, the Current Mode regulation is not directly applicable in the SLSR converter. For example, the peak value of the resonant current does not correspond to the maximum stored energy in the resonant loop.

In contrary to the hard-switching converter, the SLSR converter shows output characteristics similar to a current source as shown in [1,2]. In this case, the internal variable is more proper to be the resonant capacitor voltage v_c which reflects proportionally the integrated resonant current during each half-period of switching. The value of this variable will correspond to the size of the energy circulating in the resonant tank. The commutation command will be produced when the measured resonant capacitor voltage becomes equal to a previously calculated value $v_c(t_1)$, if this calculation guarantees (predicts) the final value v_{cmax2}. From the regulation point of view, the only controllable variable that the power switches can commutate is the current through the transistors. In the same time, by controlling the current conduction, the transistors control the charge of the resonant capacitor. The total

energy cannot be easily obtained in every moment, but it can be measured in the points of resonant current zero crossings.

The SLSR converter keeps its steady-state operation during many switching periods if there is no variation of the load and no change of the input power source values. In that case the v_{cmax1} and v_{cmax2} are equal and transistor must switch off at:

$$v_c(t_1) = qv_{c\max} \qquad (3)$$

The plots in Fig.9 illustrate the steady-state equation (3). To keep the amplitudes of the resonant capacitor voltage v_{cmax} unchanged, it is necessary to keep the switching off at its level defined by (3). The regulation method will require a calculation by multiplying the normalized output voltage q and the last measured amplitude voltage of the resonant capacitor.
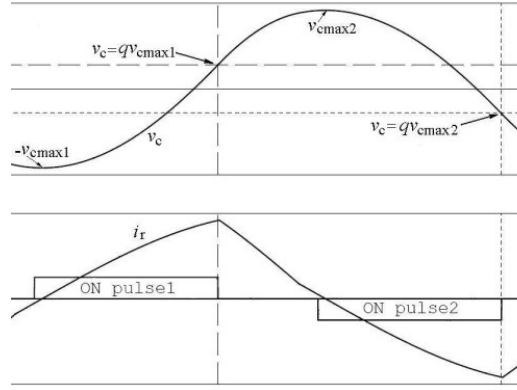

Fig. 9. Switching off of the resonant current in SLSR converter

The transition process from a lower output power consumed in an initial steady-state, to a higher level of output power, will require several portions of additional energy supplied by the resonant tank. The amplified error voltage (proportional to the difference between the really obtained and the required output voltage) will define the necessary portions of energy for the transition (similarly to the Current Mode Control).

A higher consumption of power at the output corresponds to a positive increment $\Delta \mathscr{E}_{LC}$ in the energy portions. The control action is to produce the turn-off of the transistor (or diagonal) at a certain level $v_c(t_1)_{new}$ that will be higher (added normalized energy $\Delta \mathscr{E}_{LC}^N$) than the value $qv_{c\max1}$, necessary for the steady-state operation:

$$v_c(t_1)_{new} = qv_{c\max1} + \Delta \mathscr{E}_{LC}^N = qv_{c\max2} \qquad (4)$$

The expression (4) can be simplified in order to suit better the practical implementation. The (normalized) energy increment $\Delta \mathscr{E}_{LC}^N$ is further expressed in (5) as a voltage increment $\Delta v_{c\max 1}$:

$$v_c(t_1)_{new} = q v_{c\max 1} + q \Delta v_{c\max 1} = q(v_{c\max 1} + \Delta v_{c\max 1}) \qquad (5)$$

The calculation of (5) consists in memorizing the amplitude value of the resonant capacitor voltage $v_{c\max 1}$. This value is kept until the next amplitude is read, i.e. $v_{c\max 2}$. During this "hold" time the value $v_{c\max 1}$ is multiplied by q. After that the voltage $q\Delta v_{c\max}$ (proportional to the output voltage error signal) is added. The calculated level $v_c(t_1)_{new}$ is delivered to the comparator. When the resonant capacitor voltage reaches the reference $v_c(t_1)_{new}$ the transistor current is switched off similarly to the process illustrated by Fig.9. After the switching-off the resonant capacitor voltage is expected to reach the new amplitude value $v_{c\max 2}$. The process is limited by the already developed previous v_c waveform, so the maximum $v_c(t_1)_{new}$ value (delivered to the comparator) cannot be higher than the initial value $v_{c\max 1}$. This means that the full transition process will need several half periods (at their maximum stretch).
This method is better described and simulations are proposed and tested in [10].

6 Experimental Verification

A pre-existent autonomous electric vehicle, property of HOLOS SA., was used in tests. Its power demands are lower than 250W. This relatively small vehicle is equipped with 2 sets of batteries, each one corresponding to 24V and 12Ah. The robot electric charge is made with the conventional solution which includes wires. The idea is to adopt contactless charging in the near future.

The converter applied for the test was based on a ready-made MOSFET converter for piezoelectric actuators rated 2kW, produced by APRONEX Ltd. [13]. The experimented power circuit (Fig.10) is slightly different from the shown in Fig.5, since it is based on a half-bridge structure. The half-bridge topology should be in this case more convenient considering the necessity for resonant capacitor voltage measurements, but seen from another point of view, the resonant current is supplied by two different sources alternatively: the filter capacitor C1 and filter capacitor C5. Those two power sources do not guarantee symmetry in the circuit functioning as any asymmetry in the (steady-state) process of energy exchange through the LC link is reflecting in asymmetrical charge of the filter capacitors and hence in more asymmetry.

In each half period during the time interval t_1 (from Fig.8), electrical charge is taken from one of the filter capacitors, but some part of the same charge is returned to the other filter capacitor during t_2. The result is fluctuation of the voltage in K (Fig.10) in relation to the bipolar supply voltage (310V) and some difficulty in defining the proper values of the resonant capacitor voltage.
The converter transformer (Main Transformer in Fig.10) was rebuilt in the laboratory especially to be used in contactless charging of vehicles and has relatively low magnetic coupling. Fig.11 shows the assembly achieved and the waveforms obtained.
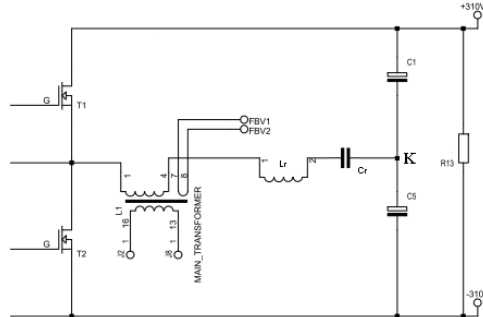
Fig. 10. Resonant converter power stage (from APRONEX Ltd.)

The fact that magnetic coupling coefficient is lower than 1 in contactless energy transfer must be consider in the transformer design. Moreover it is important to minimize the abrupt fall of magnetic coupling with the slightly misalignment that will probably occur between the primary and the secondary sides of the transformer.
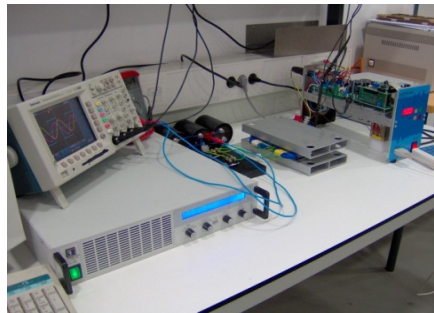

Fig. 11. Complete laboratory assembly with APRONEX MOSFET converter already modified

A conic shaped transformer (as in Fig.15) was considered as a solution to align the robot (and the secondary in it) with the primary on the floor or applied in a wall. The electric vehicle would have installed a 'nose' and the docking would take place naturally if the primary winding was itself a cone placed, for example, in a wall. The magnetic coupled obtained was too low and the idea was abandoned. Planar windings were then adopted. Planar ferrites were glued in aluminum rectangular tubes to support the windings. Aluminum here intends to absorb magnetic field leaks as a measure of protection. Fig.12 shows the primary side of the transformer with 27 turns. The secondary is similar, but it is built with 3 turns (9:1).
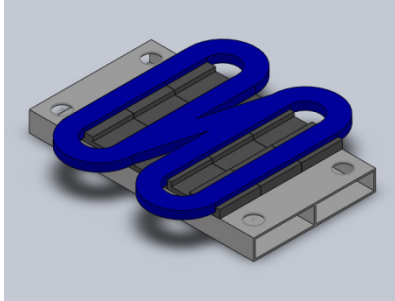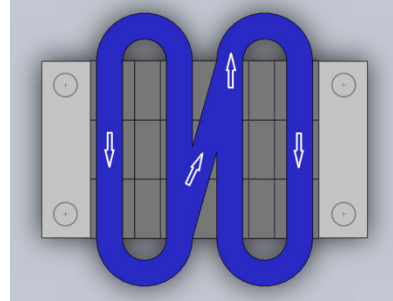
Fig. 12. Project of primary winding

Fig. 13. Primary winding with arrows indicating current direction and sense

Fig.13 shows arrows indicating the current sense. This '8' direction intends to create a magnetic arc perpendicular to the plates so the misalignment of the transformer will be less problematic.
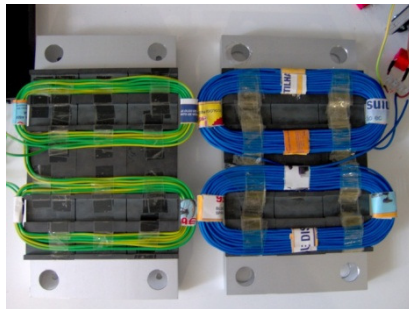

Fig. 14. Secondary and primary windings respectively in yellow/green and blue
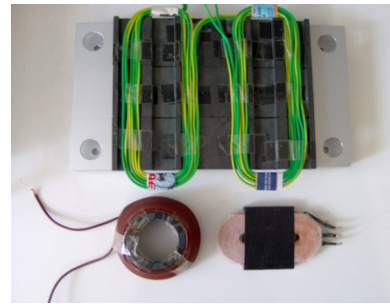

Fig. 15. Comparison between the new solution and previously adopted geometries

In the near future tridimensional simulations will be presented. New winding shapes will be tested with the main objective of increase the magnetic coupling. The converter transformer final result is visible in Fig.14. It is working well but in the near future will be improved by the supplied by APRONEX Litz wire.

A new converter (full bridge) is expected also to be supplied from APRONEX or built in the laboratory in the near future. This will improve the voltage and current shapes shown in Fig.16. The undesirable inductances of the connection cables and the slow response of the intrinsic anti-parallel diodes of the MOSFETs contributed to some flawed waveform of the current (inductive jumps in the measurements).

Regardless of all the difficulties in measuring the state variables, the obtained results are conclusive in proving the idea of instantaneous (energy balanced) control. In Fig.16 are illustrated the waveforms measured in the resonant tank. The moment in which the current i(L) is switched from the transistor to the opposite anti-parallel diode is marked by the arrow. This switching is also well visible because of the

inductive reaction of the measuring device (voltage jump). The supply voltage, i.e. the voltage on each of the double filter capacitors has a value of $v_s = 115V$. The output voltage is $v_o = 11,6V$, as the measured value from the electronic load shows in Fig.17.
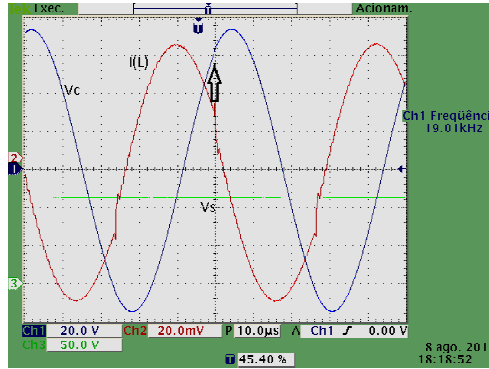

Fig. 16. Measured waveforms of the resonant converter: Vc, i(L) and input (supply) voltage Vs
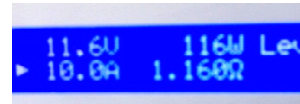
Fig. 17. Output voltage and power shown by electronic load

The transformer ratio (if it were ideally coupled transformer) should correspond to the number of turns of the primary winding divided by the secondary winding turns, i.e. 9:1. It should be expected the normalized output voltage q to be then $q = \dfrac{9x11,6V}{115V} = 0.907$. The transformer here is not ideal. The maximum coupling is obtained by maximal approximation between the primary and secondary ferrite plates and is roughly $k = 0.95$. In this case the non-ideal magnetic coupling transforms the normalized voltage in q^T [9,10], i.e.: $q^T = q.k = 0.907 * 0.95 = 0.865$. Following (3), the resonant capacitor voltage at the switching off moment must be $v_c(t_1) = q v_{c\max} = $ 0.865*74V=64V. In fact the moment of switching off is at a capacitor voltage of 64 volts.

7 Conclusions

Because of the meaning already attributed to the expression "voltage-mode" control in the past, the presented above method was called "instantaneous" control of the resonant (SLSR) converters. It permits the internal processes of the SLSR converter to be controlled faster and with precision. This control of the SLSR converter shows in experiments the good results that the simulation has shown in [10]. In case of contactless energy converter the control permits to include the magnetic coupling coefficient as another variable, observed and included into calculation. It is also possible to obtain the magnetic coupling value by other means, which will be subject of another article. Although the essence of the method of operation is similar to the Current Mode Control applied in the hard switching converters, here the internal variable (resonant voltage) must be calculated in advance (each half-period) and used

for "predictive" regulator of power. As it is shown in [1] the resonant capacitor voltage is a reliable measure for the (rectified) average resonant current.

The circuit considered above and shown in Fig.5, is unidirectional, i.e. no flow of energy is possible from the output to the input. Thus, being incapable to reduce rapidly the charge of the output (filter) capacitor by reversing the flow of energy, the shown above versions (Fig.5 and all that follow it) are not so fast in reducing the output voltage. The output voltage is only reduced by the consumption of the load. This is not a problem because even this method of regulation has sufficiently faster reaction (at least equal to the classic CM control). In case of additional controllability of the secondary (receiver) side, this method of control will be even faster.

References

1. Valtchev, S., Klaassens, J.B.: Efficient Resonant Power Conversion. In: IEEE Trans. IE, vol.37, No.6, pp. 490--495, 1990
2. Valtchev, S.: Some Regulation Characteristics of Pulse–Width Modulated Series Resonant Power Conversion. In: PEMC, Conf. Proc., pp. 83--87, Budapest, Hungary, Oct. 1990
3. Nguyen V., Dhyanchand, J.: An Implementation of Current-Mode Control for a Series-Resonant DC-DC Converter. In: APEC, Conf. Proc., pp. 266--273, 1987
4. Nguyen V., Lee, C.: A Tracking Control Method for Series-Resonant Converter. In: PESC, Conf. Proc., pp. 348--353, 1998
5. Rossetto, L.: A Simple Control Technique for Series Resonant Converters. In: IEEE Trans. PE, vol.11, No.4, pp. 554--560, 1996
6. Souesme, B., Cheron, Y., Metz, M.: Study of a Control Method to Gain the Best Dynamic Performances of the Series Resonant Converter. In: EPE, Conf. Proc., pp. 1041--1047, 1989
7. Kim, M., Lee, D.S., Youn, M.J.: A New State Feedback Control of Resonant Converters. In: IEEE Trans. IE, vol.38, No.3, pp. 173--179, 1991
8. Li, H. L., Hu, A.P., Covic, G.A.: FPGA Controlled High Frequency Resonant Converter for Contactless Power Transfer. In: PESC'08, Conf. Proc., pp. 3642--3647, 2008
9. Valtchev, S., Brandisky, K., Borges, B., Klaassens, J.B.: Resonant Contactless Energy Transfer with Improved Efficiency. In: IEEE Trans. PE, vol. 24, No. 3, pp. 685--699, 2009
10. Valtchev, S., Valtchev, S.: Improved Strategy for an Instantaneous Super-Resonant Converter Regulation. In: OPTIM 2010, pp. 631--638, 2010
11. Ridley, R.B.: A New Continuous-Time Model for Current-Mode Control. In: IEEE Trans. PE, pp. 271--280, April, 1991
12. Dias, J.V., Kim, H., Jang, D.: Computer model for railway inductive power supply using Valtchev model. In: Electrical Machines and Systems (ICEMS), 2011 International Conference, DOI: 10.1109/ICEMS.2011.6073510, pp. 1--6, 2011
13. APRONEX Ltd., High Frequency Generator for piezoelectric actuators, Gabrovo, Bulgaria, 2010